A two-degree-of-freedom piezoelectric energy harvester with stoppers for achieving enhanced performance

Guobiao Hu[1], Lihua Tang[1], Raj Das[2], and Pier Marzocca[2]*

[1]*Department of Mechanical Engineering, University of Auckland, Auckland 1010, New Zealand*

[2]*School of Engineering, RMIT University, GPO Box 2476, Melbourne, VIC 3001, Australia*

Abstract

Environmental vibrations often exist in a broadband form. To have a robust performance over a wide frequency range, vibration energy harvesters need to be designed to be insensitive to excitation frequencies. In this paper, we propose a novel two-degree-of-freedom (DOF) piezoelectric energy harvester (PEH) with stoppers that introduce nonlinear dynamic interaction between the two DOFs. First, the mechanical model of the 2DOF system with stoppers is developed by emulating the impact behaviour as a piecewise linear stiffness and the working principle is explained. Subsequently, the analytical solution of the system with piecewise linear stiffness is derived using the averaging method and the dynamic response of the system is obtained and confirms its wide bandwidth property. Finally, by integrating the mechanical system with a piezoelectric transducer, the energy harvesting performance of the proposed 2DOF PEH with stoppers is numerically evaluated. The open circuit voltage response of the proposed system is compared with that of the conventional linear 2DOF and 1DOF PEHs. A parametric study reveals the effect of the stopper distance on the energy harvesting performance in terms of both the bandwidth and open circuit voltage output. The superiority of the proposed system in terms of both power output and operation bandwidth is demonstrated.

***Keywords*:** Vibration based energy harvesting; Linear and nonlinear systems; Piecewise function; Averaging method; Piezoelectric; Two degrees of freedom.

1. Introduction

Recent advances of low-power microelectromechanical systems open the possibility of directly employing energy harvesters as power supplies and getting rid of electrochemical batteries. Therefore, energy harvesting has attracted significant research interests in recent years [1-4]. Vibration energy harvesters [2] convert and harness energy from vibrations that exist ubiquitously in industries and our daily life. Among various energy harvesting

*Corresponding author. Address: School of Engineering, RMIT University, GPO Box 2476, Melbourne, VIC 3001, Australia. Tel: +61 3 9925 6061, E-mail: pier.marzocca@rmit.edu.au

approaches, i.e., piezoelectric, electromagnetic and electrostatic transductions, piezoelectric energy harvesting has gained much attention due to its high efficiency [5-10].

Considering that environmental vibrations often exist with broad spectra, vibration energy harvesters need to be designed to be insensitive to excitation frequencies in order to have a robust performance over a wide frequency range. Therefore, the operating bandwidth [11] and the conversion efficiency [12] (i.e., the power output amplitude) naturally constitute the two main concerns in the design of vibration energy harvesters. Traditional linear vibration energy harvesters are only efficient near their resonant frequencies and quite sensitive to the variation of external excitation frequencies [13, 14]. Even a bit mis-match between the frequencies often leads to a significant deterioration of the energy harvesting performance. The power extracted in off-resonance conditions is actually quite small for practical use.

Researchers have explored various ways to improve the energy harvesting performance in terms of the operating bandwidth [13, 14]. Kim, Jung [15] designed a two degree-of-freedom (DOF) energy harvesting device that uses both the translational and rotational degrees of freedom of the proof mass. By tuning the system parameters, the two peaks in power response can get closer and thus an increased operating bandwidth can be achieved. Tang and Yang [16] introduced a multi-DOF piezoelectric energy harvester (PEH) concept. Through attaching some delicately tuned small oscillators to a 1DOF energy harvester, multiple peaks in power response can be obtained with negligible sacrifice of power density. Aldraihem and Baz [12] enhanced the power output and increased the bandwidth simultaneously by connecting the conventional PEH to a dynamic magnifier. Based on the same idea, Zhou, Penamalli [17] investigated a PEH with multi-modes. Both simulation and experimental results showed that the power output of the harvester can be magnified at multiple resonant frequencies. The aforementioned research is all based on the multi-modal concept. Other researchers revealed the usefulness of nonlinearity to enhance wideband energy harvesting [10, 13, 18]. Tang and Yang [19] proposed a nonlinear PEH by introducing a magnetic interaction between the energy harvesting beam and a magnetic oscillator. Both simulation and experimental results demonstrated the increase of the operating bandwidth of the nonlinear energy harvester. Soliman, Abdel-Rahman [20] first proposed achieving wideband vibration energy harvesting by introducing a stopper to create impacts with the mechanical system. However, although the operation bandwidth was increased, the amplitude of the peak in voltage frequency response was decreased. Based on a similar idea, Liu, Lee [21] also increased the operating frequency bandwidth of the traditional 1DOF PEH by introducing

mechanical stoppers. To extend this idea, Liu, Cheng [22] recently proposed a 2DOF PEH with a stopper, in which, the piezoelectric transducer was coupled with the primary oscillator, the stopper was installed on the base in a way that the impact may occur between the primary mass and the stopper during vibrations. Such configuration may cause problem in practical use since we always prefer that the harvester has all the components included in a standalone device rather than some components on the base. Both analytical and experimental results showed that their proposed 2DOF PEH exhibited wider operation bandwidth but the power output amplitude was decreased. Other investigations of impact engaged nonlinear systems for energy harvesting performance are reported in [23-26].

In this paper, an impact engaged 2DOF PEH with a new arrangement of mechanical stoppers is proposed. Different from all the impact engaged energy harvesters studied in the existing literature, instead of placing stoppers on the base [20-22, 25], we propose to place the stoppers onto the body with primary DOF, which introduces different dynamics worth exploring for broadband response. First, the mechanical model of the proposed system is developed using a piecewise linear stiffness function to emulate the impact behaviour during vibrations. The working principle of the potentially enhanced dynamic motion and the extended frequency response is qualitatively explained in prior to an analytical study. Then, the analytical solution to the piecewise linear model is derived by using the averaging method. The obtained frequency response of the system confirms the impact engaged nonlinear behaviour and their benefits for broadband performance. Subsequently, the mechanical system is integrated with a piezoelectric transducer, that is, the electromechanical model is built and the energy harvesting performance is numerically evaluated. The open circuit voltage output of the impact engaged 2DOF PEH is compared with that of the conventional linear 2DOF and 1DOF counterparts. The comparisons demonstrate that the new impact engaged 2DOF energy harvester can not only generate more energy output under the same excitation condition, but also exhibit a wider operation bandwidth. A parametric study is then conducted to investigate the effect of the stopper distance on the open circuit voltage output. At last, power output comparisons also confirm the superiority of the proposed impact engaged 2DOF PEH.

2. Conceptual mechanical model and theoretical analysis

2.1. Governing equations

The schematic of the proposed impact engaged 2DOF system is illustrated in Figure 1, where m_1 and m_2 represent the oscillator masses; k_1 and k_2 are the suspension spring stiffnesses; K denotes the stiffness of the stopper which is fixed onto the primary oscillator mass m_1.

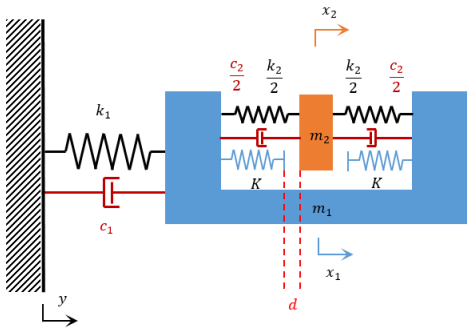

Figure 1. Schematic of a 2DOF mechanical system with stoppers

The governing equations of this 2DOF piecewise linear system can be written as:

$$\begin{cases} m_1\ddot{x}_1 + c_1\dot{x}_1 + k_1x_1 + c_2\left(\dot{x}_1 - \dot{x}_2\right) + k_2\left(x_1 - x_2\right) + p\left(x_1, x_2\right) = -m_1\ddot{y} \\ m_2\ddot{x}_2 + c_2\left(\dot{x}_2 - \dot{x}_1\right) + k_2\left(x_2 - x_1\right) - p\left(x_1, x_2\right) = -m_2\ddot{y} \end{cases} \tag{1}$$

where x_1 and x_2 denote the relative displacements to the base of the primary oscillator mass m_1 and the secondary oscillator mass m_2, respectively; y denotes the absolute displacement of the base; $p\left(x_1, x_2\right)$ is the nonlinear force associated with the impacts and can be expressed as,

$$p\left(x_1, x_2\right) = \begin{cases} K\left(x_1 - x_2 + d\right) & \left(x_1 - x_2 < -d\right) \\ 0 & \left(-d \le x_1 - x_2 \le d\right) \\ K\left(x_1 - x_2 - d\right) & \left(x_1 - x_2 > d\right) \end{cases} \tag{2}$$

where d denotes the stopper distance. This piecewise linear stiffness function emulates the impact behaviour between the two oscillator masses: the change in the spring stiffness happens when impacts occur. As shown in Figure 2, x represents the distance between m_1 and m_2. The interaction force between m_1 and m_2 is $f\left(x\right)$. When the relative distance between m_1 and m_2 is less than d, the interaction force is $f\left(x\right) = k_2\left(x_1 - x_2\right)$; once the relative distance between m_1 and m_2 exceeds d, the interaction force becomes $f\left(x\right) = k_2\left(x_1 - x_2\right) + p\left(x_1, x_2\right)$. For simplicity, the collisions between the secondary mass and the stoppers are assumed to be completely elastic and the impact induced damping is excluded.

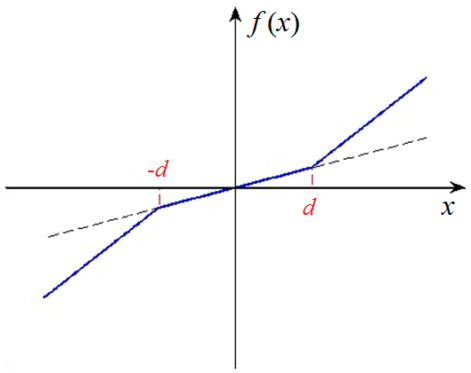

Figure 2. Piecewise linear stiffness for emulating stopper behaviour

By defining following parameters: $\omega_{10}=\sqrt{k_1/m_1}$, $\omega_{20}=\sqrt{k_2/m_2}$, $\varepsilon=K/k_1$; $\mu=m_2/m_1$; $\zeta_1=\dfrac{c_1}{2\sqrt{k_1m_1}}$, $\zeta_2=\dfrac{c_2}{2\sqrt{k_2m_2}}$, the governing equations can be rearranged as follows:

$$\begin{cases}\ddot{x}_1+2\zeta_1\omega_{10}\dot{x}_1+\omega_{10}^2x_1+2\mu\zeta_2\omega_{20}\left(\dot{x}_1-\dot{x}_2\right)+\mu\omega_{20}^2\left(x_1-x_2\right)+\varepsilon\omega_{10}^2g\left(x_1,x_2\right)=-\ddot{y}\\ \ddot{x}_2+2\zeta_2\omega_{20}\left(\dot{x}_2-\dot{x}_1\right)+\omega_{20}^2\left(x_2-x_1\right)-\dfrac{\varepsilon}{\mu}\omega_{10}^2g\left(x_1,x_2\right)=-\ddot{y}\end{cases} \tag{3}$$

$$g\left(x_1,x_2\right)=\begin{cases}\left(x_1-x_2+d\right) & \left(x_1-x_2<-d\right)\\ 0 & \left(-d\le x_1-x_2\le d\right)\\ \left(x_1-x_2-d\right) & \left(x_1-x_2>d\right)\end{cases} \tag{4}$$

2.2. Working principle

The 2DOF linear system is described by the two governing equations:

$$\begin{cases}m_1\ddot{x}_1+k_1x_1+k_2\left(x_1-x_2\right)=-m_1\ddot{y}\\ m_2\ddot{x}_2+k_2\left(x_2-x_1\right)=-m_2\ddot{y}\end{cases} \tag{5}$$

Its two natural frequencies can be easily calculated as:

$$\omega_1^2,\omega_2^2=\frac{\left(k_2m_1+\left(k_1+k_2\right)m_2\right)\mp\sqrt{\left(k_2m_1+\left(k_1+k_2\right)m_2\right)^2-4m_1m_2k_1k_2}}{2m_1m_2} \tag{6}$$

Supposing the base excitation to be in the harmonic form, by adopting Fourier transform, the displacement amplitude ratio between the secondary and the primary masses is given by:

$$r(\omega)=\frac{X_2}{X_1}=\frac{m_2k_1+m_2k_2+m_1k_2-\omega^2m_1m_2}{m_1k_2+m_2k_2-\omega^2m_1m_2} \tag{7}$$

in which X_1 and X_2 are the amplitudes of mass m_1 and m_2, respectively. Substituting the calculated frequencies ω_1 and ω_2 from Eq.(6) into Eq.(7), the displacement amplitude ratios for two vibration modes can be obtained. It can be shown that for the first mode, the

motions of the two oscillators are in phase with each other, i.e., $r(\omega_1) > 0$; while for the second mode, the motions of the two oscillators are out of phase, i.e., $r(\omega_2) < 0$. For given parameters with $m_1 = 0.056\,\text{kg}$, $m_2 = 0.0084\,\text{kg}$, $k_1 = 1500\,\text{N/m}$, $k_2 = 144\,\text{N/m}$ (damping ratios $\zeta_1 = 0.01$, $\zeta_2 = 0.006$), the displacement responses of the system around the first natural frequency and the second natural frequency are shown in Figure 3(a) and (b) respectively for a demonstration of the above phenomena.

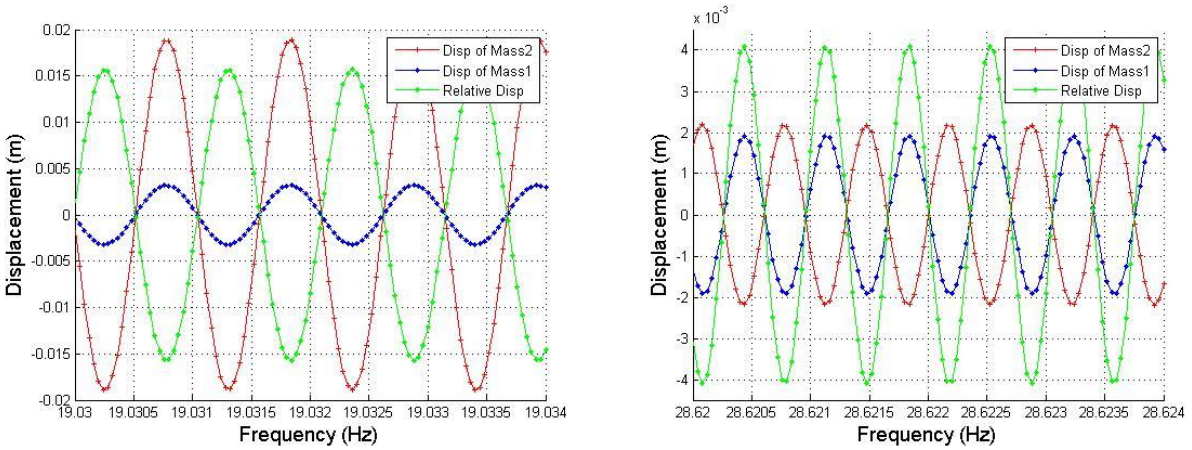

(a) (b)

Figure 3. Dynamic responses of: (a) in-phase motion around first mode; and (b) out-of-phase motion around second mode

From the perspective of energy harvesting, the motion of the piezoelectric coupled oscillator is expected to be as intense as possible. Based on the in-phase motion feature of the two oscillators, it is proposed here to create impacts between the two oscillators around the first natural frequency. To achieve this, stoppers are installed onto the primary oscillator mass m_1 in a manner so that the secondary counterpart may be able to collide with them when the relative displacement between the primary and the secondary masses becomes large enough during vibrations around the first natural frequency. In this way, it can be speculated that when they collide with each other during the in-phase motion, i.e., moving towards the same direction, the secondary mass will give a positive impulse to the primary mass. Thus the primary mass will undergo a more vigorous motion due to the additional energy imparted by the secondary mass during the impact. Therefore, by attaching the piezoelectric transducer to the primary oscillator, more energy output can be expected to be obtained. Similarly, it can be also speculated that if the impact happens during the out-of-phase motion, a negative impulse will be given to the primary mass by the secondary mass, as they move in the opposite

directions. This will in turn result in a suppression of the dynamic motion of the primary oscillator. Therefore, considering that the energy harvesting performance is closely related to the dynamic motion of the primary oscillator, it is suggested to tune the stoppers to avoid impacts to occur during the out-of-phase motion, i.e., around the second natural frequency range.

By introducing the stoppers, one can infer that by coupling a piezoelectric transducer with the primary oscillator, a higher power output is expected to be extracted. At the same time, as mechanical stoppers can induce impacts and introduce hardening nonlinear behaviour, the frequency response is expected to be extended to the high frequency range beyond the linear resonance, implying a broadband operation ability.

3. Analytical solution

3.1. Dimensionless modelling

Suppose that the base excitation is harmonic, $y(t)=Y\cos(\omega t)$. By defining the following dimensionless parameters: $u_1=\frac{x_1}{Y}$, $u_2=\frac{x_2}{Y}$, $\alpha=\frac{\omega_{20}}{\omega_{10}}$, $\Omega=\frac{\omega}{\omega_{10}}$, $\tau=\omega_{10}t$, $\delta=\frac{d\omega_{10}^2}{A}$, the dimensionless governing equations are obtained as follows

$$\begin{cases}\dfrac{d^2u_1}{d\tau^2}+2\zeta_1\dfrac{du_1}{d\tau}+u_1+2\mu\alpha\zeta_2\left(\dfrac{du_1}{d\tau}-\dfrac{du_2}{d\tau}\right)+\mu\alpha^2\left(u_1-u_2\right)+\varepsilon h\left(u_1,u_2\right)=\Omega^2\cos\left(\Omega\tau\right)\\ \dfrac{d^2u_2}{d\tau^2}+2\alpha\zeta_2\left(\dfrac{du_2}{d\tau}-\dfrac{du_1}{d\tau}\right)+\alpha^2\left(u_2-u_1\right)-\dfrac{\varepsilon}{\mu}h\left(u_1,u_2\right)=\Omega^2\cos\left(\Omega\tau\right)\end{cases} \tag{8}$$

$$h\left(u_1,u_2\right)=\begin{cases}\left(u_1-u_2+\Omega^2\delta\right) & \left(u_1-u_2<-\delta\right)\\ 0 & \left(-\delta\le u_1-u_2\le\delta\right)\\ \left(u_1-u_2-\Omega^2\delta\right) & \left(u_1-u_2>\delta\right)\end{cases} \tag{9}$$

Let $\tilde{u}_1=u_1$ and $\tilde{u}_2=u_1-u_2$. The governing equations become:

$$\begin{cases}\dfrac{d^2\tilde{u}_1}{d\tau^2}+2\zeta_1\dfrac{d\tilde{u}_1}{d\tau}+\tilde{u}_1+2\mu\alpha\zeta_2\dfrac{d\tilde{u}_2}{d\tau}+\mu\alpha^2\tilde{u}_2+\varepsilon h\left(\tilde{u}_2\right)=\Omega^2\cos\left(\Omega\tau\right)\\ \dfrac{d^2\tilde{u}_2}{d\tau^2}+2\alpha\zeta_2\dfrac{d\tilde{u}_2}{d\tau}+\alpha^2\tilde{u}_2+\dfrac{\varepsilon}{\mu}h\left(\tilde{u}_2\right)+2\zeta_1\dfrac{d\tilde{u}_1}{d\tau}+\tilde{u}_1+2\mu\alpha\zeta_2\dfrac{d\tilde{u}_2}{d\tau}+\mu\alpha^2\tilde{u}_2+\varepsilon h\left(\tilde{u}_2\right)=0\end{cases} \tag{10}$$

$$h(\tilde{u}_2)=\begin{cases}(\tilde{u}_2+\Omega^2\delta) & (\tilde{u}_2<-\delta)\\ 0 & (-\delta\le\tilde{u}_2\le\delta)\\ (\tilde{u}_2-\Omega^2\delta) & (\tilde{u}_2>\delta)\end{cases} \tag{11}$$

3.2. Frequency response

The averaging method [27] is used to derive the analytical solution to this model. The solution is assumed to be in the form as:

$$\tilde{\boldsymbol{u}}(\tau)=\boldsymbol{a}\cos(\Omega\tau-\boldsymbol{\theta}) \tag{12}$$

where the amplitude vector $\boldsymbol{a}$ and the phase angle vector $\boldsymbol{\theta}$ are both slow varying variables with respect to dimensionless time τ. Along with the assumption:

$$\dot{\tilde{\boldsymbol{u}}}(\tau)=-\boldsymbol{a}\Omega\sin(\Omega\tau-\boldsymbol{\theta}) \tag{13}$$

Eq.(12) and Eq.(13) imply:

$$\begin{cases}\dot{a}_1\cos(\Omega\tau-\theta_1)+a_1\dot{\theta}_1\sin(\Omega\tau-\theta_1)=0\\ \dot{a}_2\cos(\Omega\tau-\theta_2)+a_2\dot{\theta}_2\sin(\Omega\tau-\theta_2)=0\end{cases} \tag{14}$$

Substituting Eq.(12) and Eq.(13) into Eq.(10) yields:

$$\begin{cases}\dot{a}_1\sin(\Omega\tau-\theta_1)-a_1\dot{\theta}_1\cos(\Omega\tau-\theta_1)\\ =\dfrac{1}{\Omega}\left\{\begin{array}{l}-2\zeta_1 a_1\Omega\sin(\Omega\tau-\theta_1)+(1-\Omega^2)a_1\cos(\Omega\tau-\theta_1)\\ -2\mu\alpha\zeta_2 a_2\Omega\sin(\Omega\tau-\theta_2)+\mu\alpha^2 a_2\cos(\Omega\tau-\theta_2)+\varepsilon h(\tilde{u}_2)-\Omega^2\cos(\Omega\tau)\end{array}\right\}=f_1\\ \dot{a}_2\sin(\Omega\tau-\theta_2)-a_2\dot{\theta}_2\cos(\Omega\tau-\theta_2)\\ =\dfrac{1}{\Omega}\left\{\begin{array}{l}-2\alpha\zeta_2 a_2\Omega\sin(\Omega\tau-\theta_2)+(\alpha^2-\Omega^2)a_2\cos(\Omega\tau-\theta_2)+\dfrac{\varepsilon(1+\mu)}{\mu}h(\tilde{u}_2)\\ -2\zeta_1 a_1\Omega\sin(\Omega\tau-\theta_1)+a_1\cos(\Omega\tau-\theta_1)-2\mu\alpha\zeta_2 a_2\Omega\sin(\Omega\tau-\theta_2)\\ +\mu\alpha^2 a_2\cos(\Omega\tau-\theta_2)\end{array}\right\}=f_2\end{cases} \tag{15}$$

Solving Eq.(14) and Eq.(15) for $\dot{a}_1$, $\dot{a}_2$, $\dot{\theta}_1$ and $\dot{\theta}_2$, one obtains:

$$\begin{cases}\dot{a}_1=f_1\sin\phi_1\\ \dot{\theta}_1=-\dfrac{1}{a_1}f_1\cos\phi_1\\ \dot{a}_2=f_2\sin\phi_2\\ \dot{\theta}_2=-\dfrac{1}{a_2}f_2\cos\phi_2\end{cases} \tag{16}$$

where $\phi_1 = \Omega\tau - \theta_1$ and $\phi_2 = \Omega\tau - \theta_2$. Since $\dot{a}_1$, $\dot{a}_2$, $\dot{\theta}_1$ and $\dot{\theta}_2$ are considered to be slowly varying parameters, it can be assumed that their average values remain constant over a cycle period of 2π:

$$\begin{cases} \dot{a}_1 = \dfrac{1}{2\pi}\displaystyle\int_0^{2\pi} f_1 \sin\phi_1 d\phi_1 = \dfrac{1}{2\pi\Omega}\begin{Bmatrix} -2\zeta_1 a_1\Omega\pi - 2\mu\alpha\zeta_2 a_2\Omega\pi\cos(\theta_1-\theta_2) - \mu\alpha^2 a_2\pi\sin(\theta_1-\theta_2) \\ +\Omega^2\pi\sin\theta_1 + \varepsilon a_2\left[2\phi_0\sin(\theta_2-\theta_1) - \sin(2\phi_0)\sin(\theta_2-\theta_1)\right] \end{Bmatrix} \\ \dot{\theta}_1 = -\dfrac{1}{2\pi}\displaystyle\int_0^{2\pi}\dfrac{1}{a_1} f_1\cos\phi_1 d\phi_1 = -\dfrac{1}{2\pi a_1\Omega}\begin{Bmatrix} \left(1-\Omega^2\right)a_1\pi - 2\mu\alpha\zeta_2 a_2\Omega\pi\sin(\theta_1-\theta_2) + \mu\alpha^2 a_2\pi\cos(\theta_1-\theta_2) \\ -\Omega^2\pi\cos\theta_1 + \varepsilon a_2\left[2\phi_0\cos(\theta_2-\theta_1) - \sin(2\phi_0)\cos(\theta_2-\theta_1)\right] \end{Bmatrix} \\ \dot{a}_2 = \dfrac{1}{2\pi}\displaystyle\int_0^{2\pi} f_2\sin\phi_2 d\phi_1 = \dfrac{1}{2\pi\Omega}\left\{-2(1+\mu)\alpha\zeta_2 a_2\Omega\pi - 2\zeta_1 a_1\Omega\pi\cos(\theta_2-\theta_1) - a_1\pi\sin(\theta_2-\theta_1)\right\} \\ \dot{\theta}_2 = -\dfrac{1}{2\pi}\displaystyle\int_0^{2\pi}\dfrac{1}{a_2} f_2\cos\phi_2 d\phi_1 = -\dfrac{1}{2\pi a_2\Omega}\begin{Bmatrix} \left((1+\mu)\alpha^2 - \Omega^2\right)a_2\pi + \dfrac{\varepsilon(1+\mu)}{\mu}a_2\left[2\phi_0 - \sin(2\phi_0)\right] \\ -2\zeta_1 a_1\Omega\pi\sin(\theta_2-\theta_1) + a_1\pi\cos(\theta_2-\theta_1) \end{Bmatrix} \end{cases} \tag{17}$$

in which $\phi_0 = \arccos(\delta/a_2)$. For the steady-state response solution of the system, $\dot{a}_1$, $\dot{a}_2$, $\dot{\theta}_1$ and $\dot{\theta}_2$ are considered to be zero. Hence the following relations are obtained:

$$\begin{cases} \underbrace{-2\mu\alpha\zeta_2 a_2\Omega\pi}_{r_1}\cos(\theta_2-\theta_1) + \underbrace{\left(\mu\alpha^2 a_2\pi + 2\varepsilon a_2\phi_0 - \varepsilon a_2\sin(2\phi_0)\right)}_{r_2}\sin(\theta_2-\theta_1) + \underbrace{\Omega^2\pi\sin\theta_1}_{r_3}\underbrace{-2\zeta_1 a_1\Omega\pi}_{r_4} = 0 \\ \underbrace{\left(\mu\alpha^2 a_2\pi + 2\varepsilon a_2\phi_0 - \varepsilon a_2\sin(2\phi_0)\right)}_{r_5}\cos(\theta_2-\theta_1) + \underbrace{2\mu\alpha\zeta_2 a_2\Omega\pi}_{r_6}\sin(\theta_2-\theta_1) \underbrace{-\Omega^2\pi\cos\theta_1}_{r_7} + \underbrace{\left(1-\Omega^2\right)a_1\pi}_{r_8} = 0 \\ \underbrace{2\zeta_1 a_1\Omega\pi}_{r_9}\cos(\theta_2-\theta_1) + \underbrace{a_1\pi\sin(\theta_2}_{r_{10}}-\theta_1) + \underbrace{2(1+\mu)\alpha\zeta_2 a_2\Omega\pi}_{r_{11}} = 0 \\ \underbrace{a_1\pi\cos(\theta_2}_{r_{12}}-\theta_1)\underbrace{-2\zeta_1 a_1\Omega\pi}_{r_{13}}\sin(\theta_2-\theta_1) + \underbrace{\left((1+\mu)\alpha^2 - \Omega^2\right)a_2\pi + \dfrac{\varepsilon(1+\mu)}{\mu}a_2\left[2\phi_0 - \sin(2\phi_0)\right]}_{r_{14}} = 0 \end{cases} \tag{18}$$

By eliminating θ_1 and θ_2, two implicit equations describing the relations between dimensionless amplitudes (a_1, a_2) and dimensionless angular frequency (Ω) are obtained:

$$\begin{cases} \left(\dfrac{r_9 r_{14} - r_{11} r_{12}}{r_{10} r_{12} - r_9 r_{13}}\right)^2 + \left(\dfrac{r_{10} r_{14} - r_{11} r_{13}}{r_9 r_{13} - r_{10} r_{12}}\right)^2 = 1 \\ \left[\dfrac{1}{r_3}\left(-r_4 - r_1\dfrac{r_{10} r_{14} - r_{11} r_{13}}{r_9 r_{13} - r_{10} r_{12}} - r_2\dfrac{r_9 r_{14} - r_{11} r_{12}}{r_{10} r_{12} - r_9 r_{13}}\right)\right]^2 + \left[\dfrac{1}{r_7}\left(-r_8 - r_5\dfrac{r_{10} r_{14} - r_{11} r_{13}}{r_9 r_{13} - r_{10} r_{12}} - r_6\dfrac{r_9 r_{14} - r_{11} r_{12}}{r_{10} r_{12} - r_9 r_{13}}\right)\right]^2 = 1 \end{cases} \tag{19}$$

3.3. Analytical results

From Eq.(19), the frequency response of the displacement for the primary mass m_1 can be calculated. The frequency response of an example system with selected dimensionless parameters of $\mu = 0.15$, $\alpha = 0.8$, $\zeta_1 = 0.01$, $\zeta_2 = 0.006$, $\delta = 80$, $\varepsilon = 10$ is demonstrated in Figure 4. The parameters are carefully selected to make the impacts to occur around the first mode. It can be noted that the amplitude of the first peak is higher than its linear counterpart and shifts towards higher frequency, but the second peak in the frequency response is unchanged. It is worth mentioning that in the existing literature, the introduction of stoppers always leads to suppressed frequency response curves [20-22]. In the proposed configuration by installing stoppers onto the primary DOF member rather than the base, the introduction of stoppers, on the contrary, leads to an enhanced frequency response curve, as compared to the linear 2DOF counterpart. For the model with same dimensionless parameters ($\mu = 0.15$, $\alpha = 0.8$, $\zeta_1 = 0.01$, $\zeta_2 = 0.006$, $\delta = 80$, $\varepsilon = 10$), a simulation has been conducted. A broadband chirp excitation is applied and upward frequency sweep is performed. The comparison in Figure 4 shows that, in general, the numerical simulation result agrees well with the analytical prediction and thus establishes the benefit of the proposed configuration. It should be mentioned that the response is not an exact steady-state response during the chirp excitation, and as a result some non-smooth part in the response curve is expected when impacts occur.

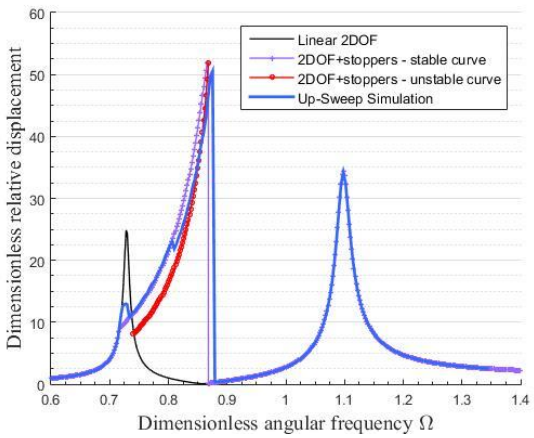

Figure 4. Analytical solution and numerical simulation of dimensionless relative displacement of primary mass m_1 of proposed system as compared to that of linear 2DOF system

4. Energy harvesting performance evaluation

4.1. Electromechanical model

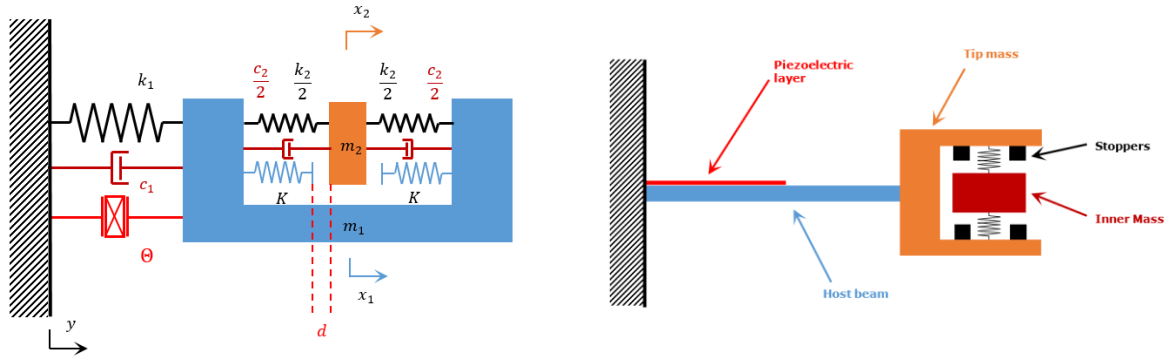

(a) (b)

Figure 5. (a) Schematic of proposed 2DOF PEH with stoppers; and (b) conceived practical prototype

Based on the above phenomenon in the impact engaged 2DOF system, by attaching a piezoelectric transducer with the primary oscillator of the 2DOF system proposed in Section 3, one can expect to obtain an energy harvester with both enhanced power output and operation bandwidth. Figure 5(a) and (b) show the schematic and the conceived practical prototype, respectively. The electromechanical governing equations of the proposed energy harvesting system can be modified as:

$$\begin{cases} m_1\ddot{x}_1 + c_1\dot{x}_1 + k_1x_1 + c_2\left(\dot{x}_1 - \dot{x}_2\right) + k_2\left(x_1 - x_2\right) + p\left(x_1, x_2\right) + \Theta v = -m_1\ddot{y} \\ m_2\ddot{x}_2 + c_2\left(\dot{x}_2 - \dot{x}_1\right) + k_2\left(x_2 - x_1\right) - p\left(x_1, x_2\right) = -m_2\ddot{y} \\ v/R + C^S\dot{v} - \Theta\dot{x}_1 = 0 \end{cases} \tag{20}$$

where Θ is the electromechanical coupling coefficient; C^S is the clamped capacitance of the piezoelectric transducer; R is the electric resistor connected to the piezoelectric transducer; and v is the voltage across R.

4.2. Open circuit output voltage and comparison

In the comparison study, parameters of the system under investigation are listed in Table 1. Under the excitation of a_{RMS} = 2 m/s^2, for a given stopper distance d = 5mm, Figure 6(a) compares the open circuit voltage responses for up-sweep of the impact engaged 2DOF energy harvesting system with that of the linear counterparts. It can be seen that the benefit of the linear 2DOF PEH is that two peaks appear in the frequency response compared with the linear 1DOF counterpart, but the appearance of the additional peak is at the sacrifice of the

voltage amplitude, resulting in an inefficient energy harvesting performance. It is worth mentioning that through carefully tuning the parameters of the secondary oscillator, one could achieve a broadband linear 2DOF energy harvester [16], while the design of such a broadband linear PEH is out of the scope of this paper. By introducing the stoppers, it can be found that the impact engaged 2DOF PEH inherited the double-peak feature of the conventional 2DOF PEH, and it is noteworthy that the amplitude of the first peak in the frequency response is significantly increased. The maximum open circuit voltage achieved by the impact engaged 2DOF PEH is about 34.48V, which corresponds to an increase in voltage of 27% and 38% as compared to those achieved by the linear 1DOF PEH (27.06V) and 2DOF PEH (24.95V), respectively. Even compared with the linear 1DOF PEH, the impact engaged 2DOF PEH exhibits a higher voltage output around the first peak. Assume the required minimal power supply voltage is 10V, the impact engaged 2DOF PEH provides a bandwidth of 5.43Hz, which means a 302% increase compared to that of the linear 1DOF PEH (i.e., 1.35Hz) or a 308% increase compared to that of the linear 2DOF PEH (i.e., 1.33Hz). However, for down-sweep, the performance of the impact engaged 2DOF PEH is deteriorated with lower peak around the first resonance and no apparent benefit in terms of bandwidth.

Table 1. System parameters

Parameters	**Physical meanings**	**Values**	**Units**
m_1	Primary oscillator mass	0.056	Kg
m_2	Secondary oscillator mass	0.0084	Kg
k_1	Primary oscillator stiffness	1500	N/m
k_2	Secondary oscillator stiffness	144	N/m
K	Stopper stiffness	15000	N/m
c_1	Primary oscillator damping	0.1833	Ns/m
c_2	Secondary oscillator damping	0.0132	Ns/m
Θ	Electromechanical coupling coefficient	1.3e-03	N/V
C^s	Capacitance	180	nF
R	Resistance	1e20	Ohm

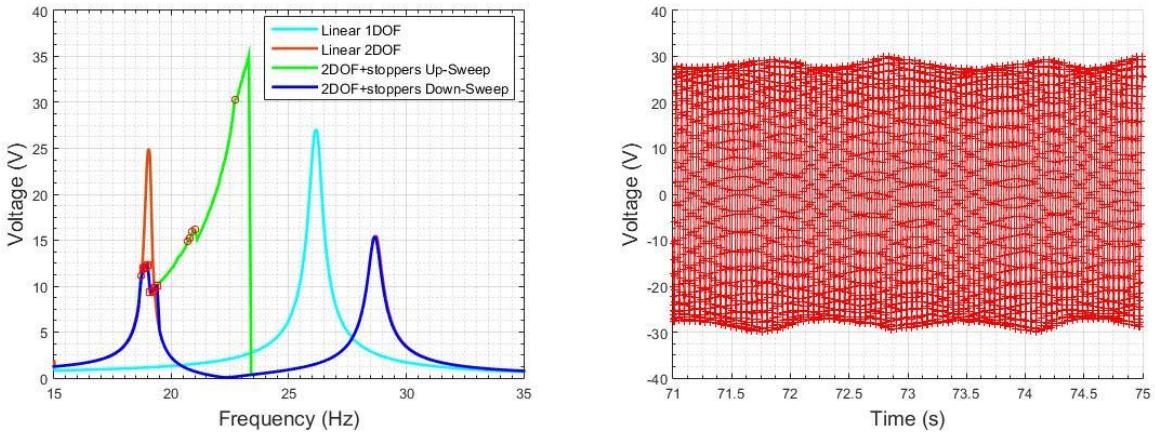

(a) (b)

Figure 6. (a) Voltage frequency response comparison of various configurations from numerical simulation; and (b) Time domain response at 22.7Hz

Based on the up-sweep simulation results, one can conclude that the impact engaged 2DOF PEH shows a relative advantage over both the conventional 1DOF and 2DOF PEHs in terms of both the open circuit voltage output and the operation bandwidth.

It is worth mentioning that the frequency responses obtained from numerical simulations shown in Figure 6(a) are not always in steady-state. At some frequencies or within some small frequency ranges (marked in red circles in Figure 6(a)), the system does not show steady state response (for example, the time domain response of the voltage at 22.7Hz shown in Figure 6(b)). Though it does not reach the steady state during the sweep simulation, the response is quite close to steady state and its contribution to energy harvesting should be considered. Therefore, considering the existence of not exact steady state responses, the maximal voltage amplitude is not a good figure of merit to characterize the system performance. Hereinafter, for the sake of fairness, the root mean square (RMS) value will be used to characterize the energy harvesting performance of the system.

4.3. Effect of stopper distance d on open circuit voltage

The stopper distance *d* plays an important role on the impact behaviour during vibrations. Therefore, this subsection studies the effect of stopper distance on the open circuit voltage output of the proposed impact engaged 2DOF PEH. Figure 7 shows the frequency responses for up-sweep of the impact engaged energy harvesting systems with different stopper distances *d*. It is found that with a decrease in the stopper distance, the amplitude of the first peak first increases then decreases. The physical explanation of this phenomenon is that with

a smaller stopper distance, the impact occurs at a position nearer to their equilibrium positions where there exist a larger speed difference between the primary and the secondary masses. Therefore, during the impact, the secondary mass imparts a larger impulse to the primary mass, leading the primary mass to undergo a more intense motion. However, when the stopper distance further significantly decreases, the relative motion of the inner oscillator will be drastically restricted which leads to a reduction in speed difference between the primary and the secondary masses. Thus, a further decrease in the stopper distance will conversely result in the decrease in the amplitude of the first peak. Besides that, with the increase of the stopper distance, the second peaks in the voltage responses for cases with different stopper distance (d =5, 7, 9, 11, 13 mm) are the same with that of the linear 2DOF counterpart. This is because the system parameters are selected in such a way so as to avoid the occurrence of impact in the frequency range around the second peak. As explained in Section 2.2, the occurrence of the impact between two oscillator masses around the second peak frequency range will lead to the suppression of dynamic motion of the primary oscillator, thus, resulting in the deterioration of the energy harvesting performance. The case of d = 3 mm shown in Figure 7 offers an example to demonstrate this. The stopper distance is reduced, so the two oscillator masses will collide with each other around the second peak frequency range. Therefore, as predicted the second peak is suppressed compared with that of the linear 2DOF counterpart.

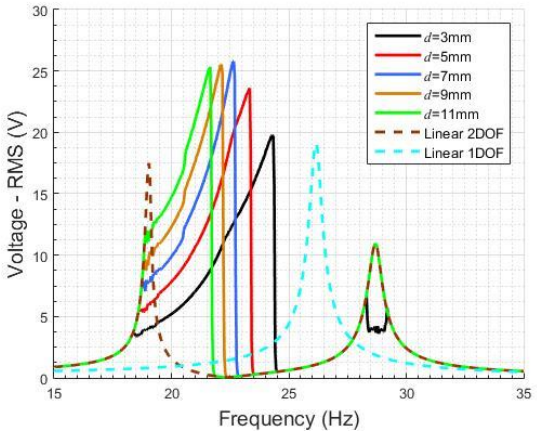

Figure 7. Voltage frequency responses from up-sweep simulation with different stopper distance d

4.4. Effect of resistance (R) on power output

The electrical circuit is also an important component that constitutes the energy harvesting system. As electromechanical coupling coefficient and the clamped capacitance of the piezoelectric transducer are inherent characters of the piezoelectric product, only the

resistance is easily customer tunable, thus only the effect of resistance on the power output of the proposed impact engaged 2DOF PEH is investigated in this section.

From Figure 7, as the case with d = 7 mm provides the highest output voltage, it is chosen to continue the following case study. Figure 8(a) and (b) show the power outputs for up-sweep of the proposed impact engaged 2DOF PEH with various resistances under weak and strong coupling conditions, respectively.

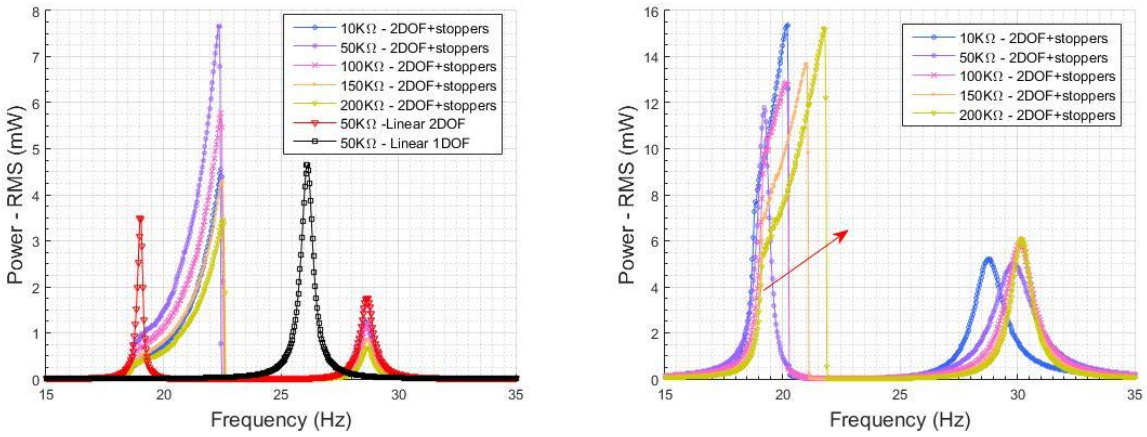

Figure 8. (a) Power output comparison of various PEH configurations for different resistances in weak coupling condition; and (b) power outputs of proposed 2DOF PEH with stoppers for different resistances in strong coupling condition

For both cases (Figure 8(a) and (b)), it is noted that the power output is quite sensitive to the resistance, to ensure a high power output, one should always select an optimal or near-optimal resistance. For the case under a weak coupling condition (Θ =1.3e-03 N/V, i.e., k_e=0.08, where the dimensionless electromechanical coupling coefficient [16] is $k_e^2 = \frac{\Theta^2}{C^S k_1}$) as shown in Figure 8(a). At the power level of 1 mW, the proposed impact engaged 2DOF PEH with near-optimal resistance of 50 kΩ provides a bandwidth of 3.82 Hz, which represents a 232.1% increase compared to the bandwidth of 1.15 Hz of the linear 1DOF and a 289.8% increase compared to the bandwidth of 0.98 Hz of the linear 2DOF PEH, respectively. The maximum power output of the proposed impact engaged 2DOF PEH with near-optimal resistance of 50 kΩ is 7.66 mW, which represents a 64.4% increase and a 118.9% increase as compared to those of the linear 1DOF PEH (i.e., 4.66 mW) and the linear 2DOF PEH (i.e., 3.50 mW), respectively. For the case under a strong coupling condition (Θ =6.6e-03N/V, k_e =0.4) as shown in Figure 8(b), besides the similar increases in bandwidth and maximum power output, one can note that with the increase of the resistance, the bandwidth of the first peak in power response of the proposed impact engaged 2DOF PEH shifts towards the right

hand side i.e., the higher frequency direction. It is noteworthy that the resistance can only have effects under strong coupling conditions, because the primary oscillator system has a resistance-dependent effective stiffness due to the existence of the piezoelectric transducer [28]. But only when the electromechanical coupling is strong, the resistance-dependent feature becomes evident.

5. Conclusions

This paper has proposed an impact engaged 2DOF PEH with a new arrangement of mechanical stoppers. The working principle of the impact engaged 2DOF mechanical system is explained and the primary oscillator system is supposed to have an enhanced dynamic motion and extended frequency response. The mathematical model of this nonlinear system is developed by emulating the impact behaviour as a piecewise linear stiffness. The analytical solution is derived by using the averaging method to obtain the frequency response of the proposed mechanical model. From the analytically calculated frequency response, the enhanced dynamic motion and extended frequency response of the primary oscillator system are confirmed. Since the energy harvesting performance is closely related to the dynamics of a mechanical system, by integrating the primary oscillator system with a piezoelectric transducer, it can be easily speculated that the proposed energy harvester can exhibit an enhanced energy output and widened operation bandwidth. According to a parametric study, the performance of the proposed impact engaged 2DOF PEH in terms of both the bandwidth and the open circuit voltage amplitude can be further enhanced by tuning the stopper distance. With a decrease in the stopper distance, the amplitude of the first peak in open circuit voltage response increases. The superiority of the proposed energy harvester over the conventional linear 2DOF and 1DOF energy harvesters is demonstrated through numerical simulations. In the selected case study, under the same conditions, the proposed impact engaged 2DOF PEH can achieve a significant increase in bandwidth and maximum power output amplitude compared to those of the linear 1DOF and 2DOF PEH. The enhancements in the bandwidths are 232.1% and 289.8% compared to those of the linear 1DOF and 2DOF PEH, respectively. The maximum power output amplitude is enhanced by 64.4% and 118.9% as compared to those of the linear 1DOF and 2DOF PEH, respectively.

Acknowledgement

This work is financially supported by the Energy Education Trust of New Zealand (no. 3708242) and the PhD scholarship from China Scholarship Council (no. 201608250001).

References

1. Priya, S. and D.J. Inman, *Energy harvesting technologies*. Vol. 21. 2009, New York: Springer.
2. Kim, H.S., J.H. Kim, and J. Kim, *A Review of Piezoelectric Energy Harvesting Based on Vibration.* International Journal of Precision Engineering and Manufacturing, 2011. **12**(6): p. 1129-1141.
3. Zhao, S. and A. Erturk, *Electroelastic modeling and experimental validations of piezoelectric energy harvesting from broadband random vibrations of cantilevered bimorphs.* Smart Materials and Structures, 2012. **22**(1): p. 015002.
4. Cha, Y., H. Kim, and M. Porfiri, *Energy harvesting from underwater base excitation of a piezoelectric composite beam.* Smart materials and Structures, 2013. **22**(11): p. 115026.
5. Kim, M., J. Dugundji, and B.L. Wardle, *Efficiency of piezoelectric mechanical vibration energy harvesting.* Smart Materials and Structures, 2015. **24**(5): p. 055006.
6. Erturk, A. and D.J. Inman, *Issues in mathematical modeling of piezoelectric energy harvesters.* Smart Materials and Structures, 2008. **17**(6): p. 065016.
7. Yang, Z., A. Erturk, and J. Zu, *On the efficiency of piezoelectric energy harvesters.* Extreme Mechanics Letters, 2017.
8. Erturk, A. and D.J. Inman, *A distributed parameter electromechanical model for cantilevered piezoelectric energy harvesters.* Journal of Vibration and Acoustics, 2008. **130**(4): p. 041002.
9. Upadrashta, D., Y. Yang, and L. Tang, *Material strength consideration in the design optimization of nonlinear energy harvester.* Journal of Intelligent Material Systems and Structures, 2015. **26**(15): p. 1980-1994.
10. Leadenham, S. and A. Erturk. *Harmonic Balance Analysis and Experimental Validation of a Nonlinear Broadband Piezoelectric Energy Harvester for Low Ambient Vibrations*. in *ASME 2015 International Design Engineering Technical Conferences and Computers and Information in Engineering Conference*. 2015. American Society of Mechanical Engineers.
11. Zhu, D., M.J. Tudor, and S.P. Beeby, *Strategies for increasing the operating frequency range of vibration energy harvesters: a review.* Measurement Science and Technology, 2009. **21**(2): p. 022001.
12. Aldraihem, O. and A. Baz, *Energy harvester with a dynamic magnifier*. Journal of Intelligent Material Systems and Structures, 2011: p. 1045389X11402706.
13. Daqaq, M.F., et al., *On the Role of Nonlinearities in Vibratory Energy Harvesting: A Critical Review and Discussion.* Applied Mechanics Reviews, 2014. **66**(4): p. 040801.
14. Tang, L., Y. Yang, and C.K. Soh, *Broadband Vibration Energy Harvesting Techniques*, in *Advances in Energy Harvesting Methods*, N. Elvin and A. Erturk, Editors. 2013, Springer New York: New York, NY. p. 17-61.
15. Kim, I.-H., et al., *Broadband energy-harvesting using a two degree-of-freedom vibrating body.* Applied Physics Letters, 2011. **98**(21): p. 214102.
16. Tang, L. and Y. Yang, *A multiple-degree-of-freedom piezoelectric energy harvesting model.* Journal of Intelligent Material Systems and Structures, 2012. **23**(14): p. 1631-1647.
17. Zhou, W., G.R. Penamalli, and L. Zuo, *An efficient vibration energy harvester with a multi-mode dynamic magnifier*. Smart Materials and Structures, 2012. **21**(1): p. 015014.
18. Leadenham, S. and A. Erturk, *M-shaped asymmetric nonlinear oscillator for broadband vibration energy harvesting: Harmonic balance analysis and experimental validation.* Journal of Sound and Vibration, 2014. **333**(23): p. 6209-6223.
19. Tang, L. and Y. Yang, *A nonlinear piezoelectric energy harvester with magnetic oscillator.* Applied Physics Letters, 2012. **101**(9): p. 094102.

20. Soliman, M., et al., *A wideband vibration-based energy harvester*. journal of micromechanics and microengineering, 2008. **18**(11): p. 115021.
21. Liu, H., et al., *Investigation of a MEMS piezoelectric energy harvester system with a frequency-widened-bandwidth mechanism introduced by mechanical stoppers*. Smart Materials and Structures, 2012. **21**(3): p. 035005.
22. Liu, S., et al., *Theoretical modeling and analysis of two-degree-of-freedom piezoelectric energy harvester with stopper*. Sensors and Actuators A: Physical, 2016. **245**: p. 97-105.
23. Kim, S., et al. *Equivalent circuit model of an impact-based piezoelectric energy harvester*. in *Journal of Physics: Conference Series*. 2014. IOP Publishing.
24. Liu, H., et al., *Piezoelectric MEMS-based wideband energy harvesting systems using a frequency-up-conversion cantilever stopper*. Sensors and Actuators A: Physical, 2012. **186**: p. 242-248.
25. Liu, H., et al., *A scrape-through piezoelectric MEMS energy harvester with frequency broadband and up-conversion behaviors*. Microsystem technologies, 2011. **17**(12): p. 1747-1754.
26. Halim, M.A. and J.Y. Park, *Theoretical modeling and analysis of mechanical impact driven and frequency up-converted piezoelectric energy harvester for low-frequency and wide-bandwidth operation.* Sensors and Actuators A: Physical, 2014. **208**: p. 56-65.
27. Narimani, A., M. Golnaraghi, and G.N. Jazar, *Frequency response of a piecewise linear vibration isolator*. Journal of Vibration and control, 2004. **10**(12): p. 1775-1794.
28. Hu, G., et al., *Metastructure With Piezoelectric Element for Simultaneous Vibration Suppression and Energy Harvesting*. Journal of Vibration and Acoustics, 2016. **139**(1): p. 011012-011012-11.